

## LETTERS

The purpose of this Letters section is to provide rapid dissemination of important new results in the fields regularly covered by *Physics of Fluids*. Results of extended research should not be presented as a series of letters in place of comprehensive articles. Letters cannot exceed four printed pages in length, including space allowed for title, figures, tables, references and an abstract limited to about 100 words. There is a three-month time limit, from date of receipt to acceptance, for processing Letter manuscripts. Authors must also submit a brief statement justifying rapid publication in the Letters section.

## Apparent fluid slip at hydrophobic microchannel walls

Derek C. Tretheway and Carl D. Meinhart<sup>a)</sup>

Department of Mechanical Engineering, University of California, Santa Barbara, California 93106

(Received 23 October 2001; accepted 14 November 2001)

Micron-resolution particle image velocimetry is used to measure the velocity profiles of water flowing through  $30 \times 300 \mu\text{m}$  channels. The velocity profiles are measured to within 450 nm of the microchannel surface. When the surface is hydrophilic (uncoated glass), the measured velocity profiles are consistent with solutions of Stokes' equation and the well-accepted no-slip boundary condition. However, when the microchannel surface is coated with a 2.3 nm thick monolayer of hydrophobic octadecyltrichlorosilane, an apparent velocity slip is measured just above the solid surface. This velocity is approximately 10% of the free-stream velocity and yields a slip length of approximately  $1 \mu\text{m}$ . For this slip length, slip flow is negligible for length scales greater than 1 mm, but must be considered at the micro- and nano scales. © 2002 American Institute of Physics. [DOI: 10.1063/1.1432696]

At the macroscopic level, it is well accepted that the boundary condition for a viscous fluid at a solid wall is one of "no-slip," i.e., the fluid velocity matches the velocity of the solid boundary. While the no-slip boundary condition has been proven experimentally to be accurate for a number of macroscopic flows, it remains an assumption that is not based on physical principles. In fact, nearly two hundred years ago Navier proposed a general boundary condition that incorporates the possibility of fluid slip at a solid boundary. Navier's proposed boundary condition assumes that the velocity,  $v_x$ , at a solid surface is proportional to the shear stress at the surface<sup>1,2</sup>

$$v_x = \beta (dv_x/dy), \quad (1)$$

where  $\beta$  is the slip length or slip coefficient. If  $\beta = 0$  then the generally assumed no-slip boundary condition is obtained. If  $\beta$  is finite, fluid slip occurs at the wall, but its effect depends upon the length scale of the flow. For example, the solution for Stokes flow between two infinite parallel plates with the boundary conditions of no shear stress at the centerline and Navier's hypothesis (1) at the wall, yields

$$v_x = \frac{h^2}{2\mu} \left( -\frac{dp}{dx} \right) \left[ \left( 1 - \left( \frac{y}{h} \right)^2 \right) + \frac{2\beta}{h} \right], \quad (2)$$

where  $2h$  is the distance between the two plates,  $\mu$  is the viscosity, and  $(-dp/dx)$  is the pressure drop. The first term in the brackets,  $1 - (y/h)^2$ , is the standard solution for pressure-driven Stokes flow between two infinite parallel plates with no slip, while the second term,  $2\beta/h$ , represents

an additional velocity associated with the general boundary condition (1). The first term is of order one while the second term depends on the plate separation,  $2h$ . If  $\beta$  is finite, as  $h$  decreases, the importance of the second term increases. Thus, at the micro- and nano-length scales this term can be significant and dominate Eq. (2). Assuming Navier's hypothesis, and since the no-slip assumption appears to be valid at the macroscale,  $\beta$  must be relatively small.

Recently, several researchers have suggested that the no-slip boundary condition may not be suitable for hydrophilic flows over hydrophobic boundaries at both the micro- and nano scale. With hot-film anemometry, Watanabe *et al.*<sup>3,4</sup> identified fluid slip at the wall of a strongly hydrophobic duct or pipe. Their velocity profiles are consistent with Navier's hypotheses. However, their results are for a relatively large-scale rectangular duct ( $15 \times 15 \text{ mm}$ ) and modest Reynolds numbers. In microfluidic devices, similar Reynolds numbers cannot be achieved. Ruckenstein and Rajora<sup>5</sup> investigated fluid slip in glass capillaries with surfaces made repellent to the flowing liquid. Their experimental results of pressure drop indicate larger slip than that predicted by chemical potential theory, where slip is proportional to the gradient in the chemical potential. The results suggest that slip occurs over a gap near the surface rather than directly on the solid surface, and the gap forms when a hydrophobic liquid flows over a hydrophilic surface and vice versa. Their results, however, are inferred from pressure drop-flow measurements and not direct measurement of the fluid velocities. Computationally, Barrat and Bocquet<sup>6</sup> expect significant slip in nanoporous media when the liquid is sufficiently nonwetting. The slip increases the effective permeability of the nanoporous medium. Their predictions were experimentally justified by

<sup>a)</sup> Author to whom correspondence should be addressed. Electronic mail: meinhart@engineering.ucsb.edu

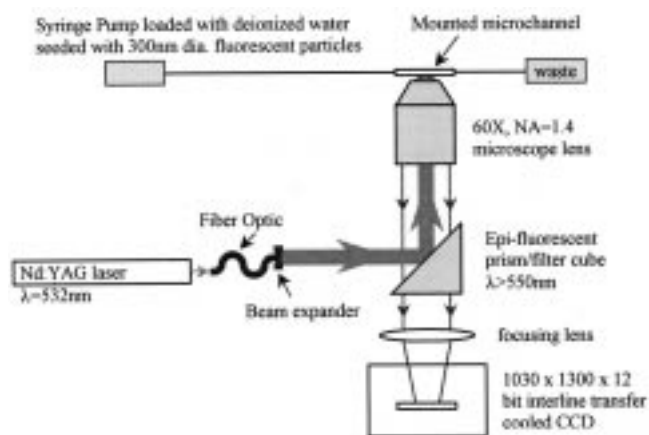


FIG. 1. Experimental micro particle image velocimetry ( $\mu$ -PIV) setup. Two frequency-doubled Nd:YAG lasers emit green light pulses separated by a time delay of  $150 \mu\text{s}$ . The pulses are directed into the inverted microscope, reflected off a filter cube, and refracted by the objective lens into the microchannel. Deionized water seeded with fluorescent particles is pumped through the microchannel. The particles absorb green light and emit red light. The red light is captured by the objective lens, passed through a long-pass filter ( $\lambda = 550 \text{ nm}$ ), and focused onto a CCD camera.

Churaev *et al.*,<sup>7</sup> who measured water flow in thin ( $< 1 \mu\text{m}$ ) hydrophobic capillaries. Zhu and Granick<sup>8</sup> experimentally observe the possibility of slip in an oscillating surface force apparatus with slip lengths (point into the wall at which the inferred velocity would go to zero) of up to  $2.5 \mu\text{m}$  for separations of  $20$ – $100 \text{ nm}$ . Their results suggest a strong dependence between the velocity gradient and magnitude of the slip. Their conclusions, however, are inferred from variations in the measured normal forces and are not measured directly. Pit *et al.*<sup>9</sup> observed fluid slip between rotating parallel disks with a gap of  $160 \mu\text{m}$ . By following the movement of a photo-bleached test section, they conclude that slip depends on the interfacial energy and surface roughness.

The current work examines the no-slip boundary condition by applying micron-resolution particle image velocimetry ( $\mu$ -PIV) to measure the flow of water in microchannels that have a clean surface (hydrophilic) and in microchannels that are coated with hydrophobic octadecyltrichlorosilane (OTS). The PIV measurements show apparent fluid slip for water flowing over a solid hydrophobic surface and no slip for a hydrophilic surface.

Figure 1 is a schematic of the micro-PIV measurement system. The pulses of two frequency-doubled Nd:YAG lasers ( $\lambda = 532 \text{ nm}$ ) are combined, directed through a fiber optic cable, and expanded into the illumination port of a Nikon Eclipse TE200 inverted microscope. The pulses are reflected by a long-pass filter cube (epi-fluorescent prism) and relayed through a  $\text{NA} = 1.4$ ,  $60\text{X}$  oil immersion objective lens into the microchannel. Fluorescently dyed  $300 \text{ nm}$  diameter flow-tracing polystyrene spheres absorb the green ( $\lambda = 532$ ) laser light and emit red ( $\lambda = 575$ ) light. The fluorescent light is imaged by the objective lens and passed through the long-pass filter, where green light from background reflection is filtered out. The remaining red light is focused by a relay lens onto a cooled  $1030 \times 1300 \times 12$  bit interline transfer CCD camera. A cooled CCD camera is required to suppress

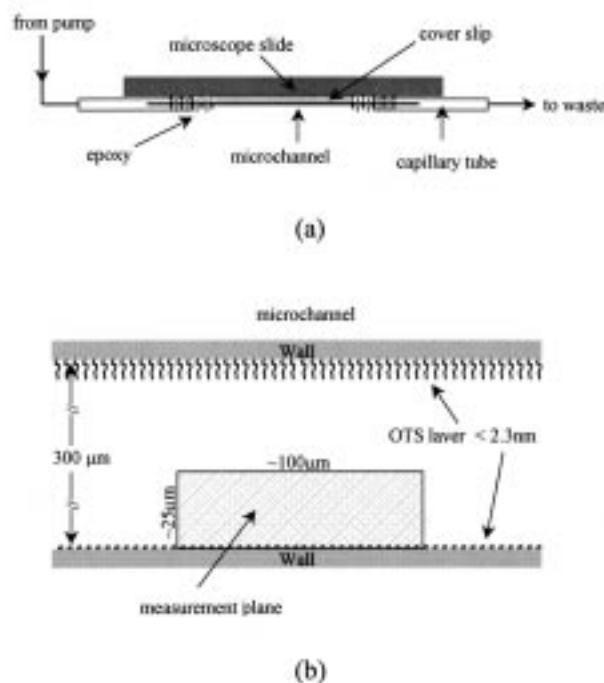


FIG. 2. (a) Diagram of the mounted microchannel. (b) Schematic of a microchannel (top view) showing the PIV measurement plane and the OTS-coated hydrophobic surface.

dark-current noise so that the low light levels emitted by the fluorescent particles can be recorded. The interline transfer feature allows back-to-back recording of two images with a minimum time delay of  $500 \text{ ns}$ . The duration of a single laser light pulse combined with the decay time of the fluorescent dye is on the order of  $5$ – $10 \text{ ns}$ , which effectively freezes the motion of the particles. The delay time between the two laser pulses is set to  $150 \mu\text{s}$ . The two images captured by the CCD camera are then analyzed with PIV software developed by Steve Wereley (currently at the Department of Mechanical Engineering, Purdue University). The interrogation region is  $128 \times 8$  pixels (streamwise by spanwise), which yields a spatial resolution of  $14.7 \times 0.9 \times 1.8 \mu\text{m}$  with velocity measurements obtained to within  $450 \text{ nm}$  of the channel wall. The out-of-plane measurement depth is approximately  $1.8 \mu\text{m}$ . To increase the signal-to-noise ratio,  $49$  image pairs are cross correlated. The resulting correlation functions are then averaged before peak detection, following the algorithm given by Meinhart *et al.*<sup>10</sup>

The velocity profiles are measured in  $30 \mu\text{m}$  deep  $\times 300 \mu\text{m}$  wide extruded glass microchannels trimmed to a length of  $8.25 \text{ cm}$ . Measurements are made  $4$  to  $4.5 \text{ cm}$  from the edge of the microchannel to eliminate entrance effects and ensure a fully developed flow profile. The microchannel is mounted on a microscope slide. A cover slip is positioned between the microscope slide and the microchannel, to displace the microchannel from the microscope slide and to provide rigid support. The ends of the microchannel are then inserted into capillary tubes. An epoxy seals the capillary tubes and binds the microscope slide, cover slip, microchannel, and capillary tubes together. The microscope slide (with the microchannel, cover slip, and capillary tubes attached) is then inverted and set into a bracket mounted to the transla-

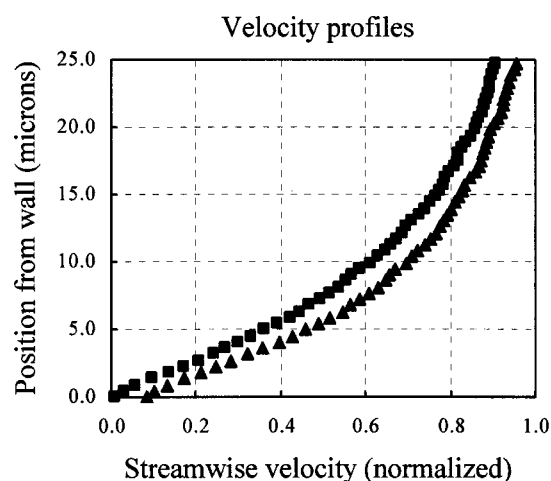


FIG. 3. Velocity profiles for flow over a hydrophilic (square) and hydrophobic (triangle) microchannel surface. The velocity profiles are normalized by the free-stream velocity.

tion stage directly above the objective lens. A diagram of the mounted microchannel is shown in Fig. 2(a). Deionized water, seeded with the 300 nm diameter fluorescent polystyrene spheres (Interfacial Dynamics Corp.), is injected into the microchannel at a constant flow rate of 200  $\mu\text{l/h}$  using a Harvard Apparatus PHD2000 syringe pump.

An untreated glass microchannel is naturally hydrophilic. Hydrophobic microchannels are created by coating the walls of the microchannel with octadecyltrichlorosilane (OTS). The untreated microchannel is first pretreated with a concentrated sodium hydroxide solution, which opens the silicon oxide layer by creating hydroxyl groups. The microchannels are then rinsed with water and dried thoroughly. The cleaned microchannel is then exposed multiple times to a 2 mM solution of OTS in dicyclohexyl for approximately one hour during each exposure. During this time, OTS reacts with the silicon atom of the exposed hydroxyl groups. The OTS reaction with silicon is autophobic, which limits the coating to a single monolayer. After the OTS exposure, the microchannels are rinsed with chloroform and dried. The microchannels are then baked at 100  $^{\circ}\text{C}$  overnight. This curing process cross links the individual OTS molecules, creating a smooth and robust monolayer. At maximum density, the OTS layer is approximately 23  $\text{\AA}$  thick with a surface roughness of 2–3  $\text{\AA}$ . The layer thickness is less than 1/10 000th the depth of the microchannel. Figure 2(b) is a schematic of a coated microchannel. Since the contact angle cannot be measured inside the microchannel, a reference section of glass is treated concurrently with the microchannels to provide an estimate of the effectiveness of the reaction. The contact angle between water and the OTS surface is estimated to be approximately 120 $^{\circ}$ . This is consistent with accepted contact angle values.

Figure 3 shows the average velocity profile for flow near the wall for hydrophilic (squares) and hydrophobic (triangles) microchannel surfaces. The velocity profiles are normalized by the free-stream velocity. Measurements are taken in the midplane of the channel (15  $\mu\text{m}$  from the bottom) near the side wall [see Fig. 2(b)]. The field of view is aligned such that a section of the wall is included in each image. Since

there are no particles in the wall, the resulting correlations for that region produce erroneous velocity vectors with magnitudes and directions that are inconsistent with the known direction of flow. The wall location is then set at the point at which the velocity vectors are erroneous. The uncertainty of wall location is approximately 450 nm.

For a hydrophilic surface (squares), Fig. 3 shows the velocity approaching its free-stream value at 25  $\mu\text{m}$  from the wall and smoothly decreasing to zero at the wall. This profile is consistent with the analytical solution for flow through a rectangular duct with a finite aspect ratio, assuming the no-slip boundary condition.<sup>11</sup> For flow through a hydrophobic microchannel, the velocity profile is significantly different. While Fig. 3 shows the hydrophobic velocity profile (triangles) near its free-stream value at 25  $\mu\text{m}$  and decreasing towards the wall, a finite and significant velocity is measured within 450 nm above the wall. This slip velocity is approximately 10% of the free-stream velocity, and effectively shifts the entire velocity profile when compared with the no-slip profile (squares). As a result, the velocity 25  $\mu\text{m}$  from the wall in a hydrophobic microchannel is approximately 95% of the free-stream velocity, compared with 90% for a microchannel that is hydrophilic. Thus, a monolayer of hydrophobic molecules with a thickness of less than 23  $\text{\AA}$  significantly affects the velocity profile even out to a distance of 25  $\mu\text{m}$  from the wall. The observed shift in the velocity profile is consistent with the results of Watanabe *et al.*,<sup>3</sup> even though their results are for a flow through a significantly larger duct and at higher Reynolds numbers.

The results of Fig. 3 provide a measurement of apparent fluid slip for water flowing over a hydrophobic surface, and confirm the no-slip boundary condition for water flowing over a hydrophilic surface. However, a number of issues remain unresolved: First, is Navier's general boundary condition (1) valid? From current measurements we calculate a slip length,  $\beta$ , of approximately 1  $\mu\text{m}$ . This is consistent with the work by Zhu and Granick,<sup>8</sup> who report slip lengths of approximately 2  $\mu\text{m}$ . Since the current experiments are limited to a narrow range of flow rates, we are unable to determine if the slip velocity is proportional to the shear stress, with  $\beta$  being a constant. Second, if we assume that the slip velocity is proportional to the shear stress, what physical phenomena determine the value of  $\beta$ ? Do solution properties (i.e., ionic concentration or surfactants) modify  $\beta$ ? Ruckenstein and Rajora<sup>5</sup> suggest that entrained or soluble gases in the flowing liquid may increase fluid slip by forming a gap between the liquid and the wall, thereby increasing  $\beta$ . The current working fluid is deionized water. Future experiments are planned using degassed water and various modified solutions to explore physical properties of the slip boundary condition.

In summary, micron-resolution particle image velocimetry was applied to measure velocity profiles of flow through 30  $\times$  300  $\mu\text{m}$  channels. We measure an apparent slip velocity at the wall for water flowing through a microchannel coated with hydrophobic OTS. This slip velocity is approximately 10% of the free-stream velocity and yields a slip length of approximately 1  $\mu\text{m}$ . For a clean, hydrophilic channel, the measured velocities are consistent with the no-slip boundary

condition. These results indicate that modeling fluid flow at the micro scale with the assumption of no-slip may not be accurate, and may depend upon the interaction between the fluid and the wall surface properties.

#### ACKNOWLEDGMENTS

This work is supported by Grant Nos. NSF CTS-9874839, NSF ACI-0086061, and DARPA/Air Force 30602-00-2-0609.

<sup>1</sup>C. L. M. H. Navier, *Mem. Acad. R. Sci. Inst. France* **1**, 414 (1823).

<sup>2</sup>S. Goldstein, *Modern Developments in Fluid Dynamics* (Dover, New York, 1965), Vol. 2, p. 676.

<sup>3</sup>K. Watanabe, Yanuar, and H. Mizunuma, "Slip of Newtonian fluids at solid boundary," *JSME Int. J., Ser. B* **41**, 525 (1998).

<sup>4</sup>K. Watanabe, Yanuar, and H. Udagawa, "Drag reduction of Newtonian fluid in a circular pipe with a highly water-repellant wall," *J. Fluid Mech.* **381**, 225 (1999).

<sup>5</sup>E. Ruckenstein and P. Rajora, "On the no-slip boundary condition of hydrodynamics," *J. Colloid Interface Sci.* **96**, 488 (1983).

<sup>6</sup>J. Barrat and L. Bocquet, "Large slip effect at a nonwetting fluid–solid interface," *Phys. Rev. Lett.* **82**, 4671 (1999).

<sup>7</sup>N. Churaev, V. Sobolev, and A. Somov, "Slippage of liquids over lyophobic solid surfaces," *J. Colloid Interface Sci.* **97**, 574 (1984).

<sup>8</sup>Y. Zhu and S. Granick, "Rate-dependent slip of Newtonian liquid at smooth surfaces," *Phys. Rev. Lett.* **87**, 096105 (2001).

<sup>9</sup>R. Pit, H. Hervet, and L. Leger, "Direct experimental evidence of slip in hexadecane: Solid interfaces," *Phys. Rev. Lett.* **85**, 980 (2000).

<sup>10</sup>C. Meinhart, S. Wereley, and J. Santiago, "A PIV algorithm for estimating time-averaged velocity fields," *J. Fluids Eng.* **122**, 285 (2000).

<sup>11</sup>F. White, *Viscous Fluid Flow* (McGraw-Hill, New York, 1974), p. 123.